Friction
Research Article

Tribology and particle emission from Al–SiCp MMC brake discs with secondary aluminum

Yezhe Lyu[1,✉], Lucia Lattanzi[2], Samuel Awe[3], Anders EW Jarfors[2], Jens Wahlström[1]

Cite this article: Lyu YZ, Lattanzi L, Awe S, et al. *Friction* 2026, **14**(7): 9441217. https://doi.org/10.26599/FRICT.2026.9441217

ABSTRACT: This study evaluated the friction, wear, and airborne brake wear particle (BWP) emissions of aluminum-based metal matrix composite brake discs fabricated from recycled aluminum alloy reinforced with silicon carbide particles (Al–SiCp MMC). The study further conducted a comparative analysis of the friction, wear, and BWP emissions of Al–SiCp MMCs against those of a commercial gray cast iron (GCI) brake disc, which served as a reference. The results show that the steady-state coefficient of friction for all Al–SiCp MMC brake discs remained consistently between 0.4 and 0.45, within the typical range for brake materials. A clear transfer layer was observed on the surfaces of Al–SiCp MMC discs after testing, resulting in apparently milder wear due to material transfer and reduced BWP emissions. Al–SiCp MMC brake discs resulted in higher wear rates for the mating pins than the GCI discs, with wear rates increasing as the fraction of secondary aluminum in the matrix increased. Within the measurement range of this study, both GCI and Al–SiCp MMC brake discs exhibited monomodal number-weighted particle size distributions in the steady state, with the mode size of approximately 0.5 μm. Future research should employ advanced particle samplers capable of detecting nanosized particles and explore more severe testing conditions, including higher contact pressures, speeds, and temperatures.

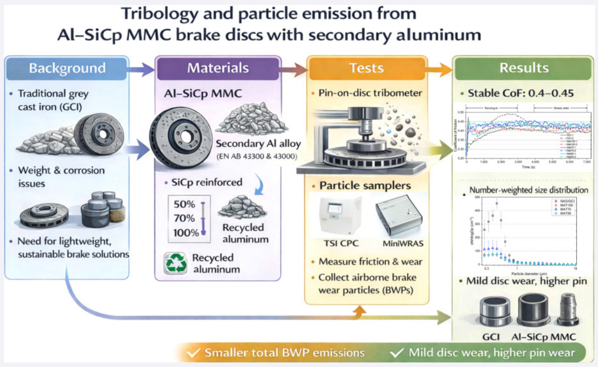

KEYWORDS: brake emission; metal matrix composite; aluminum; recycling; secondary aluminum alloys; pin-on-disc

1 Introduction

Traditional automotive brake discs are made from gray cast iron (GCI) because of its excellent castability, cost-effectiveness, and high damping capacity [1, 2]. However, its poor corrosion resistance results in thick rust layers during long periods of idleness, negatively affecting both braking capacity and visual aesthetics [3]. This challenge is more pronounced in electric vehicles, which mainly utilize the regenerative braking system. Aluminum-based metal matrix composites (Al-MMCs) have great potential to substitute GCI to produce automotive brake discs, with good tribological performance and corrosion resistance in lightweight solutions [4, 5].

Silicon carbide (SiC) particles have been one of the most extensively studied reinforcements in Al-MMCs since the 1990s [6], with this system later designated as Al–SiCp MMCs. Previous studies have investigated the effects of SiC particle size and volume fraction on the friction and wear behaviors of Al–SiCp MMCs [5, 7–9]. Sliding speed, contact pressure, and temperature have been proven to significantly affect the coefficient of friction (CoF) and wear of Al–SiCp MMC brake discs [10–18]. To overcome the softening challenge of Al–SiCp MMCs at high temperatures, reinforcing alloying elements such as Cu, Ni, Zr, Ce, and La were investigated to improve their thermal, mechanical, and tribological properties at high temperatures [19–23].

Al–SiCp MMCs have also been compared with traditional GCI brake discs regarding CoF and wear to assess their suitability for automotive brake disc applications [24–28]. Another emerging metric for automotive brake disc evaluation is the brake wear particle (BWP) emissions, which now contribute up to 21% of the total traffic-related PM10 emissions [29]. Although research on BWP emissions from GCI brake discs is extensive, there are very few published studies specifically focusing on the BWP emissions from Al–SiCp MMC brake discs [30].

Previous studies suggest that reducing vehicle weight by replacing steel and cast iron with aluminum can lead to noticeable fuel savings [31]. However, the production of primary aluminum is highly energy-consuming and results in significant greenhouse gas emissions. Fortunately, aluminum scrap can be recycled to produce secondary alloys, potentially saving up to 95% of the energy required for primary aluminum production [32]. Lattanzi et al. [33] have also succeeded in producing Al-MMC with

[1] Department of Mechanical Engineering Sciences, Lund University, Lund 223 63, Sweden. [2] Department of Materials and Manufacturing, School of Engineering, Jönköping University, Jönköping 553 18, Sweden. [3] Automotive Components Floby AB, Floby 521 21, Sweden.

✉ Corresponding author. E-mail: yezhe.lyu@mel.lth.se

Received: February 19, 2025; Revised: December 15, 2025; Accepted: January 14, 2026

secondary aluminum alloys and have investigated its thermal and mechanical properties. This method proposed a new application that can absorb end-of-life aluminum scrap. Currently, there is very limited knowledge on wear particle emissions from Al-MMC brake discs, especially the ones produced with secondary aluminum alloys. This study investigates the friction, wear, and airborne BWP emission characteristics of Al–SiCp MMC brake discs fabricated from secondary Al (EN AB 43000) and silicon carbide particles, and compares these properties with those of the conventional GCI brake rotor.

2 Experimental

2.1 Materials

This study investigated three Al–SiCp MMCs with varied fractions of secondary Al–10Si–Mg alloys (EN AB 43000) in the matrix (50%, 70%, and 100%), designated as Mat50, Mat70, and Mat100, respectively. The primary alloy EN AB 43300 (Al–9Si–Mg) was combined in a specific ratio with the secondary alloy EN AB 43000 (Al–10Si–Mg) to produce Mat50 and Mat70 metal matrix composites. All three MMCs were reinforced with 20 wt% SiC particles (targeted content), a typical SiCp fraction commonly reported in Refs. [6, 14, 15] and used in commercial products [34]. The SiC particles had an average particle size of 20 μm. The MMCs were produced using a squeeze casting technique following the procedure described in previous work [23]. An arc/spark optical emission spectrometer (SPECTROMAXx©CCD LMXM3, Spectro Analytical Instruments) was used to measure the chemical compositions of the produced Al–SiCp MMCs, as presented in Table 1. The Si content higher than 24 wt% accounts for the Si in both the matrix alloys and the reinforcing carbides.

A commercial GCI brake disc was also tested as a reference. The chemical composition of the GCI in weight percentage was 3.8% C, 1.8% Si, 0.65% Mn, 0.05% S, 0.05% P, and balanced Fe. It was reported that the conventional brake pad for mating with the GCI brake disc is not suitable for Al-MMC application due to poor braking effects and wear properties [24]. Therefore, two commercial non-asbestos organic (NAO) brake pad materials were used as counterparts in the experiments. One NAO (designated as NAO I) brake pad was specifically designed for GCI brake discs, while the other NAO (designated as NAO II) brake pad was specifically designed for Al-MMC brake discs. Both brake pad materials are commercial products, and their exact chemical compositions are confidential.

2.2 Experimental setup

A Nanovea® T50 pin-on-disc tribometer (PoD) was used to test the brake pad and disc materials (Fig. 1), which was designed according to ASTM G99 and DIN 50324 standards. The PoD contains a horizontally rotating disc and a vertically dead-weight-loaded pin. It can apply a normal load of up to 60 N and rotate at up to 5,000 $r \cdot min^{-1}$. A load cell was mounted on the side of the beam to directly measure the friction force, which was used to calculate the CoF. For the PoD experiments, the brake pads were extracted into cylindrical pin samples with a testing surface diameter of 10 mm, whilst the Al–SiCp MMC and GCI brake discs were shaped into circular disc samples with a testing surface diameter of 60 mm. The sliding speed was 2 $m \cdot s^{-1}$, and the contact pressure was 0.6 MPa for all friction pairs (Table 2). These test conditions result in temperature levels of approximately 150 °C, as measured with a sliding thermocouple in our previous study [35], which are comparable to those typically observed in vehicles operating under Los Angeles City Traffic (LACT) conditions [35, 36]. Each test lasted for 120 min to ensure a prolonged test duration. The long duration of the tests is intended to ensure that the pin-disc contact reaches a steady state, allowing for a stable and reliable brake particle emission measurement. This is commonly used in brake particle emission studies with pin-on-disc tribometers [37–39]. The main reason for the prolonged test duration is to accurately assess the brake materials' performance under steady-state conditions (i.e., stable temperature and friction coefficient), thereby reflecting their actual behavior in real applications. Wear mass loss of each test sample was measured with a Radwag® analytical balance model AS 520.R2 PLUS with a precision of 0.1 mg. Before the weight measurement, the sample surfaces were cleaned with pressurized air to remove the attached wear debris. Each friction pair was tested for two repetitions and each repetition used new pin and disc samples.

The PoD was placed in a one-way ventilated box with a unique inlet and a unique outlet. An Allentown EcoFlo™ air cleaner model EFS120GR, equipped with a class H14 HEPA filter (a high-efficiency particulate air filter with a minimum filtration efficiency of 99.995%), was connected to the inlet to provide a stable supply of particle-free air. A TSI® condensation particle counter (CPC model 3752) and a Grimm® portable wide-range aerosol spectrometer (MiniWRAS model 1371) were used to conduct the online measurements of the emitted BWP over a wide particle size range. The CPC measured particle number concentration (PNC) is within the size range of 4 nm up to 3 μm, whilst the MiniWRAS measured PNC and particle size distribution ranges from 0.01 to 35 μm. The MiniWRAS combined both electrical (0.01–0.25 μm) and optical (0.25–35 μm) techniques, measuring PNC in 41 size bins. The PNC ranges of CPC and MiniWRAS are 0–10^5 and 200–10^6 cm^{-3}, respectively.

The original microstructure of the composites before tribological testing and the wear tracks on the discs and the pins were evaluated by an optical microscope (OM; Olympus DSX1000) and a scanning electron microscope (SEM; Tescan Mira 4) using secondary electrons (SE) and back-scattered electrons (BSE) detectors. The chemical nature of different microstructural features was evaluated by an energy dispersive X-ray spectrometer (EDS; EDAX Octane Elect). Quantitative image analysis (IA) was performed with MIPAR software (version 1) to measure the area fraction of the SiC particles on 16 micrographs, each with a field of view of 200 μm × 200 μm for each material. The assumption that the area fraction is comparable to the volume fraction is common in metallurgy when sampling randomly cut planes, and the material is approximately isotropic [40]. The weight fraction f_w of the SiCp for each material was

Table 1 Chemical composition of Al–SiCp MMCs measured by arc/spark optical emission spectrometer (Unit: wt%)

Material	Secondary	Primary	Si [a]	Fe	Cu	Mn	Mg	Al
Mat50	50	50	> 24	0.23±0.01	0.58±0.17	0.05±0	0.51±0.05	Balance
Mat70	70	30	> 24	0.33±0.02	0.30±0.11	0.05±0	0.54±0.02	Balance
Mat100	100	0	> 24	0.46±0.03	0.34±0.17	0.06±0	0.55±0.04	Balance

Note: [a] The Si content includes the Si in both the matrix alloy and the SiC particles.

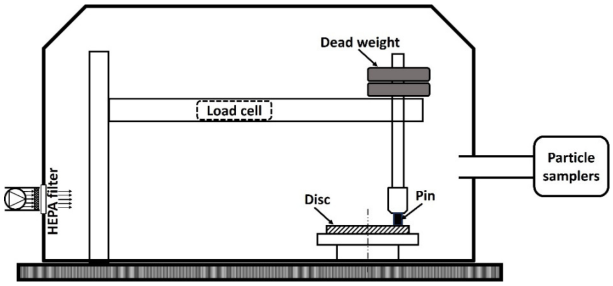

Fig. 1 Schematic of experimental setup.

estimated using Eq. (1), where f (%) is the volume fraction of the particles, d_p = 3.4 g·cm^{-3} is the density of the particles, and d_m = 2.6 g·cm^{-3} is the density of the matrix alloy.

$$f_w = \frac{f \times d_p}{f \times d_p + (1-f) \times d_m} \tag{1}$$

The theoretical density d_{RoM} of the composites was estimated using the rule of mixture (RoM) in Eq. (2).

$$d_{RoM} = f \times d_p + (1-f) \times d_m \tag{2}$$

The density d_{IA} is estimated by Eq. (2), and the fraction f is the area fraction obtained by IA, once again assuming that the area fraction is comparable to the volume fraction.

3 Results and discussion

3.1 Microstructure

Figure 2 shows the composite material's microstructure, consisting of the Al–Si matrix alloy and the dark polygonal SiC particles. Figure 2(a) shows that the SiC particles are randomly dispersed in the matrix alloy, and their area fraction in the composites ranges from 25.3% to 28.7%. The area fraction provides an overestimate of the reinforcement fraction, as shown in Table 3. Assuming that the area fraction is comparable to the volume fraction and the density of SiCp is 3.4 g·cm^{-3}, the estimated weight fractions of SiCp are in the 31–34 wt% range. Due to this overestimation in the reinforcement fraction, the density values estimated by the fraction from image analysis in Eq. (1) have an overestimation error of 2%. The related values of density calculated by the rule of mixture in Eq. (2) align well with the experimental density values measured at room temperature.

Figure 2(b) shows that the matrix alloy presents the primary Al phase (α-Al) in dendritic form, light gray, and the eutectic Si particles in the interdendritic regions. The presence of Fe and Mg determines the precipitation of different intermetallic phases, as depicted in Fig. 2(c). The Mg_2Si phase and two types of Fe-based intermetallic compounds are present in all materials. One phase always presents a thin rod-like morphology and the chemical composition of Al(Fe,Mn)Si, suggesting the δ-$Al_3(Fe,Mn)Si_2$ phase [41]. The other phase presents an irregular morphology that ranges from coarse rod to script form, with a chemical composition of AlFeMgSi, suggesting the π-$Al_8FeMg_3Si_6$ phase [42].

3.2 Friction and wear

Figure 3 shows the real-time CoF data as measured in the experiments. It can be seen from Fig. 3 that all friction pairs showed running-in periods where the CoF gradually stabilized. The durations of the running-in periods varied among different friction pairs. After the running-in, the CoF of different friction pairs reached a steady state featuring a relatively stable CoF until the end of the test run. In the running-in period, the initial surface

Table 2 Specifications for test friction pairs and conditions

Friction pair	Brake pad	Brake disc	Sliding speed (m·s^{-1})	Contact pressure (MPa)
NAO/GCI	NAO I	Gray cast iron	2	0.6
NAO/Mat50	NAO II	50% secondary aluminum Al–SiCp MMCs	2	0.6
NAO/Mat70	NAO II	70% secondary aluminum Al–SiCp MMCs	2	0.6
NAO/Mat100	NAO II	100% secondary aluminum Al–SiCp MMCs	2	0.6

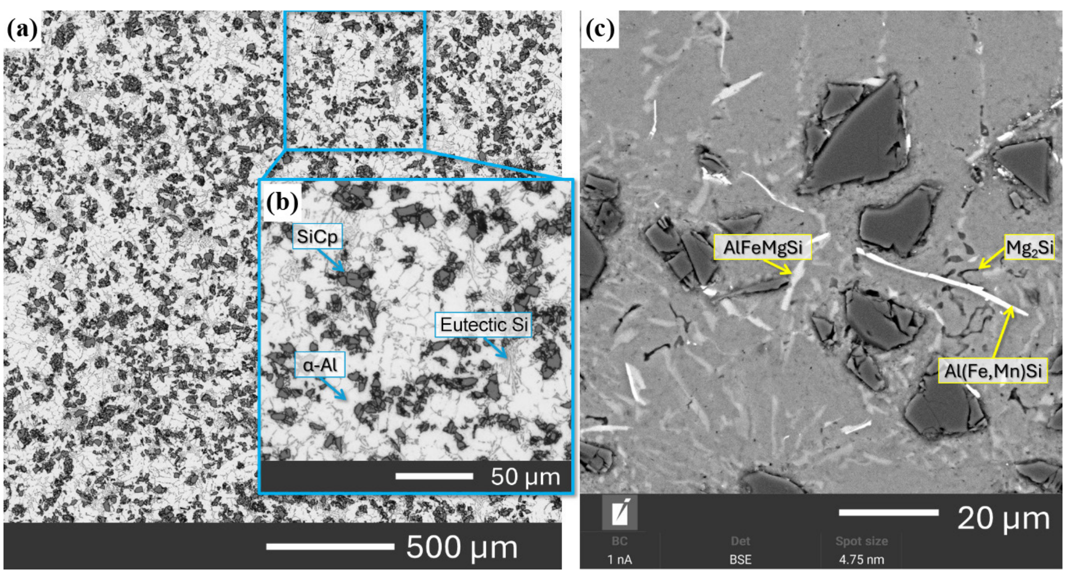

Fig. 2 Microstructure of Mat50, representative of the other MMCs regarding distribution of carbides and intermetallic phases: (a) OM panorama of SiCp distribution; (b) focus on main microstructural features; (c) SEM image (BSE detector) of intermetallic phases in matrix, identified by EDS.

Table 3 Estimated SiCp mass fraction after image analysis and density data of composites

Material	Target SiCp (wt%)	d_{RoM} (g·cm^{-3})	Area fraction of SiCp from IA (%)	Estimated SiCp (wt%)	d_{IA} (g·cm^{-3})	Measured density (g·cm^{-3})
Mat50	20	2.76	28.7±2.0	34±2	2.83±0.02	2.76±0.01
Mat70	20	2.76	26.7±1.8	32±2	2.81±0.01	2.77±0.01
Mat100	20	2.76	25.7±2.2	31±2	2.81±0.02	2.76±0.01

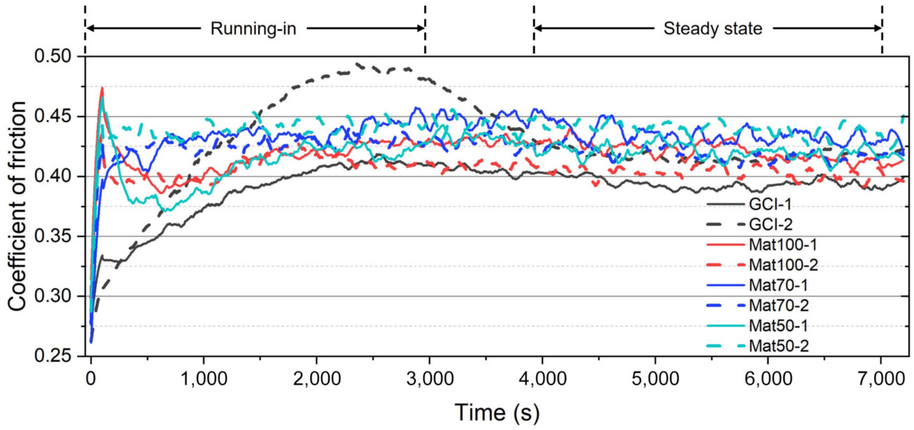

Fig. 3 Coefficient of friction as measured by load cell.

characteristics were worn off, and the pin and disc surfaces got gradually engaged with each other, finally reaching the steady state characterized by a consistent CoF. Both the GCI and Al-MMC brake discs with various secondary aluminum alloys had steady-state CoF values approximately between 0.4 and 0.45, well falling within the typical CoF range for braking materials [28]. Some previous studies have found that the average CoF of the GCI brake disc is higher than that of the Al-MMC brake disc [6, 26]. However, in these experiments, the same brake pad material was tested against both GCI and Al-MMC discs, unlike the current study, where different brake pad materials were used to pair with different brake disc materials. One advantage of Al-MMC brake discs is that their CoF is not sensitive to changes in sliding speed, unlike the GCI brake disc [8, 15, 27]. Contact pressure has been found to have a greater impact on the CoF of original Al-MMC brake discs, highlighting the importance of evaluating the CoF behavior of Al-MMC brake discs with secondary aluminum under different contact pressures [26, 27].

Figure 4 shows the specific wear rate (K_a) of the pin and disc samples across two repetitions for different friction pairs. The specific wear rate was calculated following Archard's wear law (Eq. (3)) [43].

$$K_a = \frac{\Delta m}{\rho \cdot \Delta s \cdot F_N} \tag{3}$$

where Δm is the mass loss of the sample as measured with the analytical balance; ρ is the density of the sample; Δs is the sliding distance; F_N is the applied normal load. K_a allows for evaluating wear behavior independent of differences in sample densities and normal loads. It should be noted that the K_a values correspond to the entire test duration instead of the running-in periods or steady state, as shown in Fig. 3. The sample densities used in the calculations are 2.67 g·cm^{-3} for NAO I and 2.64 g·cm^{-3} for NAO II brake pads (measured using Archimedes' principle), 7.2 g·cm^{-3} for GCI, and 2.77 g·cm^{-3} for Al–MMC brake discs.

It can be seen from Fig. 4 that the average pin wear rates seemed to gradually increase as the fraction of secondary aluminum in the Al-MMCs (Mat100 was the highest on average and Mat50 the lowest). It can also be noticed that the Al-MMC brake discs resulted in notably higher wear rates for the mating pins than the GCI brake discs. GCI brake discs had very low wear rates, and all three Al-MMC brake discs had apparently milder wear rates due to material transfer, indicating that some materials were added onto the Al-MMC surfaces after testing. The milder wear due to material transfer/surface build-up of Al-MMC brake discs has been seen in Refs. [24, 30], where a clear transfer layer was found on the Al-MMC disc surface after testing. Another noticeable phenomenon is that the pin tested against Mat100 brake discs exhibited the greatest scatter in wear rate across the two repetitions, whilst all other wear rates were highly consistent across the two repetitions. This might be attributed to the highest fraction of secondary aluminum alloys in the matrix, resulting in the greatest degradation of the thermal and mechanical properties of the Al-MMC brake discs [33]. Temperature is recognized as a significant factor influencing the wear behaviors of brake materials [10, 11], which needs to be further investigated in future studies.

3.3 Particle emission

The PNC as measured by CPC and MiniWRAS across two

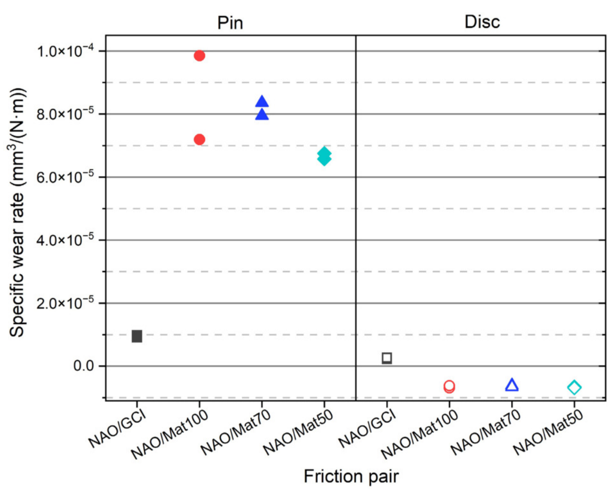

Fig. 4 Specific wear rate of tested pin and disc samples across two repetitions.

repetitions of different friction pairs is shown in Fig. 5. In each subfigure, the left *y*-axis shows the concentration as measured by CPC and designated as $PN_{4nm–3μm}$, while the right *y*-axis is the concentration as measured by MiniWRAS and designated as $PN_{0.25–10μm}$. It should be noted that the PNC below 0.25 μm, as measured by MiniWRAS, is very uncertain due to the relatively low concentration values. Therefore, the current study only included the MiniWRAS particle size range above 0.25 μm, where it utilized the optical technique, which is always reliable.

For the GCI brake disc, $PN_{0.25–10μm}$ remained a constant offset from the $PN_{4nm–3μm}$ in repetition 1 (red dots vs. red line). A similar offset was also seen in the running-in period in repetition 2 (Fig. 3). However, in the steady state of repetition 2 of the GCI brake disc, $PN_{0.25–10μm}$ and $PN_{4nm–3μm}$ were highly consistent with each other. In contrast, $PN_{0.25–10μm}$ and $PN_{4nm–3μm}$ of Al–MMC brake discs with different fractions of secondary aluminum showed high consistency in the running-in periods, whilst exhibiting a clear offset in the steady state. A possible reason might be the inhomogeneous distribution of various ingredients in the pad materials. In the brake pad, up to 20 different ingredients are mixed, which play different roles in the braking process [44]. The ingredients are sometimes not mixed homogeneously in the pad, resulting in enrichment of some ingredients in the extracted pin samples. This is likely to lead to the differences in PNC observed across the two repetitions of the same friction pair, such as Mat70 in Fig. 5. Further, $PN_{4nm–3μm}$ of GCI brake discs was constantly higher than or equal to $PN_{0.25–10μm}$ for the GCI brake discs, whilst it was the opposite for Al-MMC brake discs. It is noticeable that all Al-MMC brake discs started to generate fine particles after some running (red and black solid lines in Fig. 5). This phenomenon is different from the PNC time series reported in some literature, where the PNC showed very a high peak in the running-in period then went down to a relatively low and stable level in the steady state [35, 45]. Further study with a thermal denuder which can remove all volatile and organic aerosols should be conducted to clarify this phenomenon and explain the underlying particle formation mechanisms [46].

For a more detailed analysis, a box plot that separates the running-in and steady-state periods for $PN_{4nm–3μm}$ and $PN_{0.25–10μm}$ is presented in Fig. 6. It can be seen from Fig. 6 that all three Al-MMC brake discs have almost equal $PN_{4nm–3μm}$ and $PN_{0.25–10μm}$ in the running-in periods, indicating the generation of particles mainly within the range of 0.25–3 μm. However, in the steady state, all three Al-MMC brake discs have notably higher $PN_{4nm–3μm}$ values than $PN_{0.25–10μm}$, demonstrating clear evidence of the generation of particles below 0.25 μm. There is very little published information on airborne wear particle emissions from Al-MMCs. The only archived study has seen apparently higher concentration measured by a condensation particle counter (10 nm–3 μm particle size range) than an optical particle sizer (0.3–10 μm particle size range) at 0.9 MPa contact pressure, which was assumed to be above the critical temperature for the disc brake system [47].

For the GCI brake disc, $PN_{4nm–3μm}$ was on average lower than $PN_{0.25–10μm}$ in the running-in period and very close to that in the steady state, indicating that most of the generated particles from GCI brake discs were within the optical size range (above 0.25 μm) under the current test condition. This is in accordance with previous studies [1, 48]. In the current study, the particle mass concentration was not considered since very different particle effective densities from GCI and Al-MMC brake discs were assumed, making the particle mass concentration calculation by MiniWRAS unreliable. Future work should measure the exact effective density of the generated particles from both GCI and Al-MMC brake discs [49].

The number-weighted particle size distribution, as measured by MiniWRAS in the steady state, is plotted in Fig. 7. GCI and Al-MMC brake discs showed a monomodal size distribution with a mode size of approximately 0.5 μm. It should be noted that MiniWRAS only measured particle size range from ~0.3 μm, and particles in the nanosize range are not covered. This agrees with several previous studies on BWP emissions using different brake pad and brake disc materials [1, 50, 51]. Since there is clear evidence of particles below 0.25 μm generated from Al-MMC brake discs in the steady state (Figs. 5 and 6), further studies with a scanning mobility particle sizer, which can reach the nanosized particle range, are needed to explore the particle size distribution below 0.25 μm.

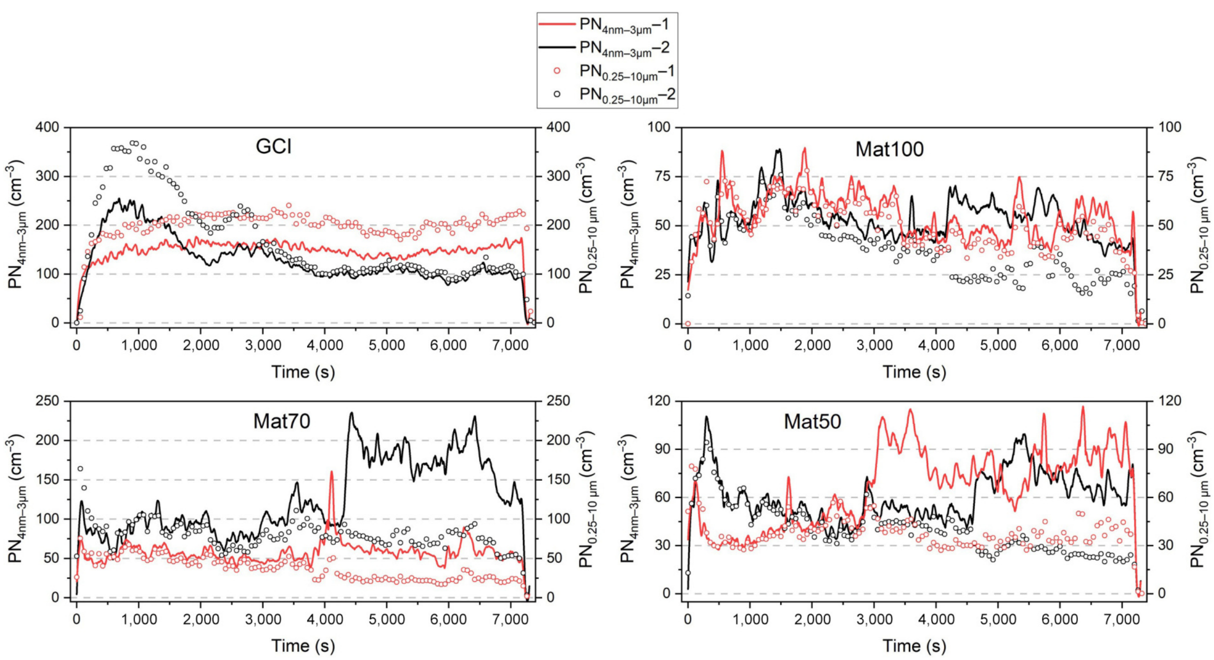

Fig. 5 PNC as measured by CPC (4 nm–3 μm, left *y*-axis in figures) and MiniWRAS (0.25–10 μm, right *y*-axis in figures) of different friction pairs.

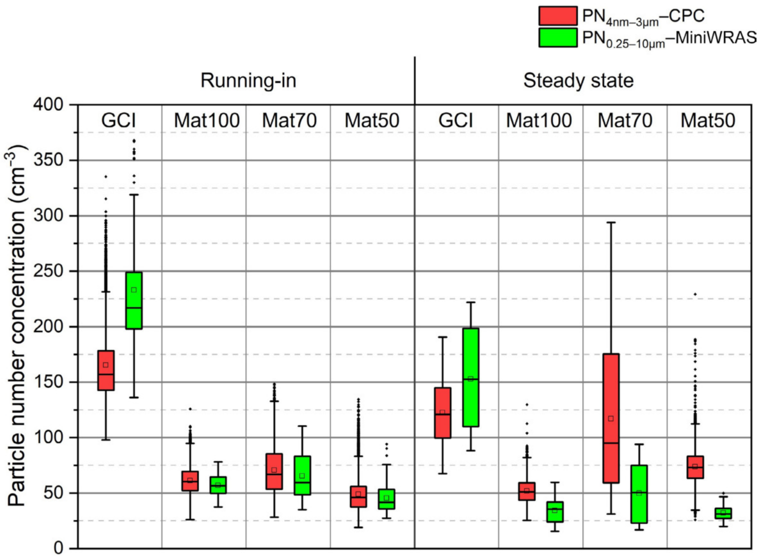

Fig. 6 Box plots of PNC in running-in period (200–3,000 s in test duration) and steady-state period (4,000–7,000 s in test duration) as measured by CPC (4 nm–3 μm) and MiniWRAS (0.25–10 μm).

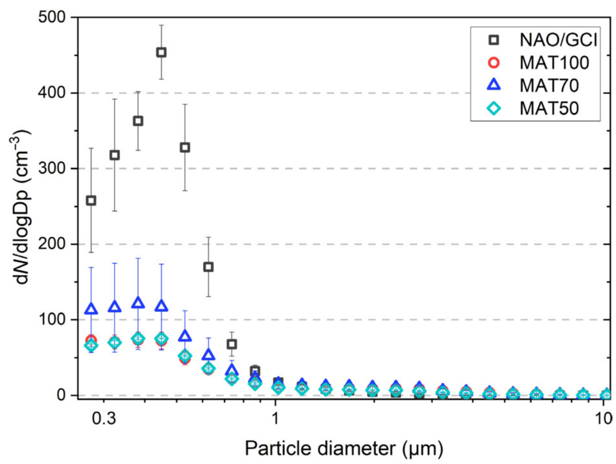

Fig. 7 Particle size distribution as measured by MiniWRAS in optical technique range (0.25–10 μm). d*N*/dlogDp represents the particle number size distribution normalized by the logarithmic particle diameter interval.

3.4 Wear tracks

The observation of the wear tracks on the disc samples highlighted a significant difference in appearance between the GCI and the Al-MMC brake discs (Fig. 8). Clear blackish transfer layers can be observed on all three Al-MMC brake discs after testing. The transfer layers were also found in a previous study on Al-MMC brake discs [30]. The SEM-observed wear track of Mat50 is presented in Fig. 9(a), representative of the other Al-MMCs as well. The surface presents islands of wear debris, bright in the SEM image, adhering to the aluminum surface, and the SiCp is visible in the areas without debris. This observation of surface build-up aligns with the milder wear of the Al-MMCs shown in Fig. 4 and the visible transfer layers shown in Fig. 8. This transfer layer built up with the wear debris might be the reason for the fewer particles emitted from Al-MMC brake discs, in comparison with the GCI brake disc. A similar built-up transfer layer which reduced particle emissions was observed on hard coatings on GCI substrates produced with high-velocity oxygen fuel technique [35]. It should be noted that the transfer layer can capture particles and reduce emissions, like in the current study, but it may also act as a source of fine particles, as seen in the "off-brake emissions peak" [52, 53]. Signs of abrasive wear parallel to the sliding directions are also visible in the aluminum matrix not covered by the debris.

The wear track appeared different on the GCI brake disc, as shown in Fig. 9(b). Abrasive wear tracks are visible on the entire surface as well as cracks that can be correlated to the graphite in the material. Wear debris deposits are visible where the crack width is enough to accommodate extra material. In the GCI case, the wear debris is in powder form and does not adhere to the surface, while on the Al-MMCs the debris is more compact and appears on top of the surface, covering a large portion of the material. This observation agrees with the wear rates shown in Fig. 4.

Figure 10 presents the EDS analysis of the wear track and

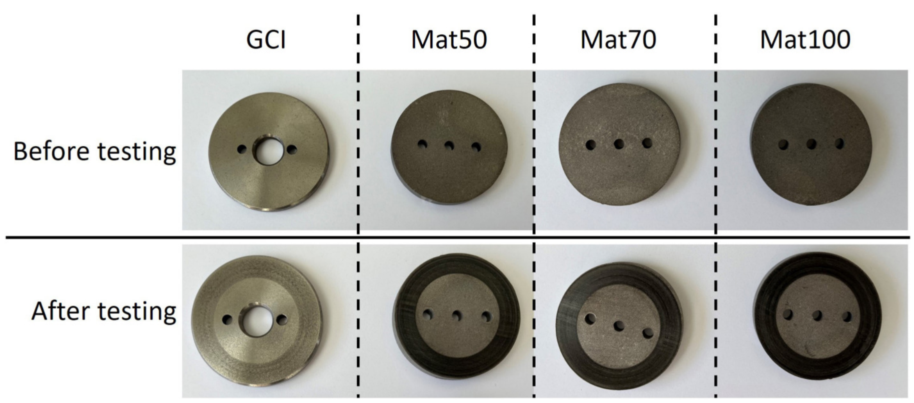

Fig. 8 Appearances of tested disc samples before and after testing.

debris of Mat70. The EDS mapping highlights that the wear debris layers, previously described as blackish transfer layers (Fig. 8), consist of oxidized material, containing carbon and magnesium. The presence of carbon in the debris is related to the phenolic resin binder of the brake pad material. Due to the lower electrical conductivity of the debris than that of the disc material (Fig. 10(a), the debris is brighter than the surrounding material in secondary electron signal micrograph), and a reliable quantitative chemical composition is not derived. The aluminum and silicon signals are related to the areas free from debris, with silicon corresponding to the SiC particles in the composite, visible on the wear track as black spots on the BSE image (Fig. 10(b)).

To further understand the material transfer between the disc and the pad, the NAO II brake pad material was investigated before and after wear testing. Figure 11(a) shows that the material consists of a phenolic resin-bonded matrix reinforced with particulate materials varying in size and composition. It is challenging to determine their chemical composition due to the analytical technique, but the EDS map suggests the presence of carbides and oxides containing Mg and Al. Figure 11(b) presents the wear track on the pin after testing against Mat100. There are tracks parallel to the sliding direction and some wear debris on the surface. Comparing Figs. 11(a) and 11(b), there is very limited material transferred from the Al-MMC brake disc to the pad during the tribological tests, due to the fact that Si and Al (elements that also exist in the Al-MMC brake discs) show no significant changes.

In summary, the investigation of the wear tracks on the discs

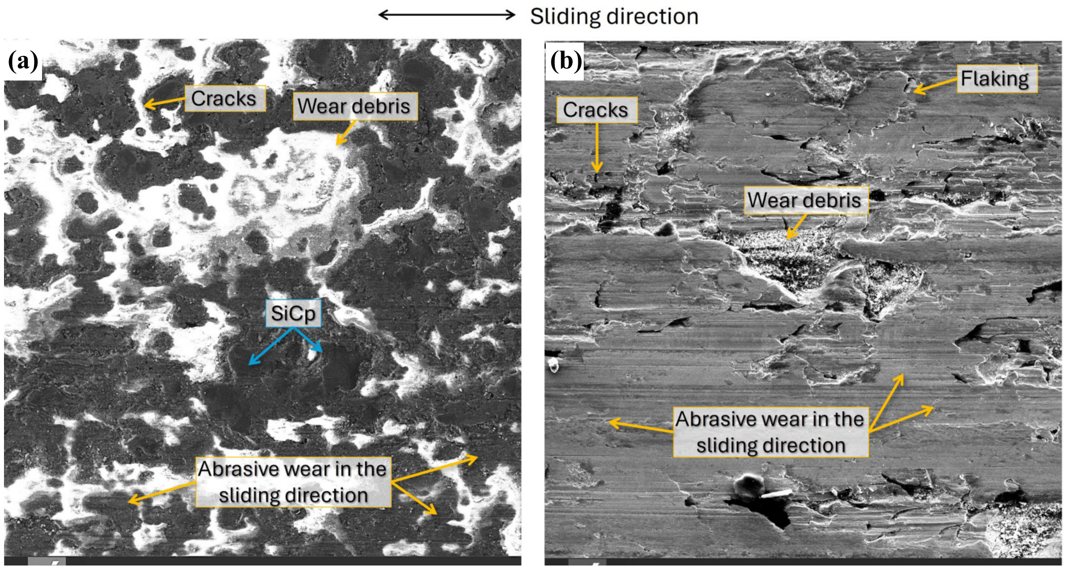

Fig. 9 SEM images (SE) of wear tracks of: (a) Mat50, representative of Al–SiCp MMC brake discs; (b) GCI brake disc.

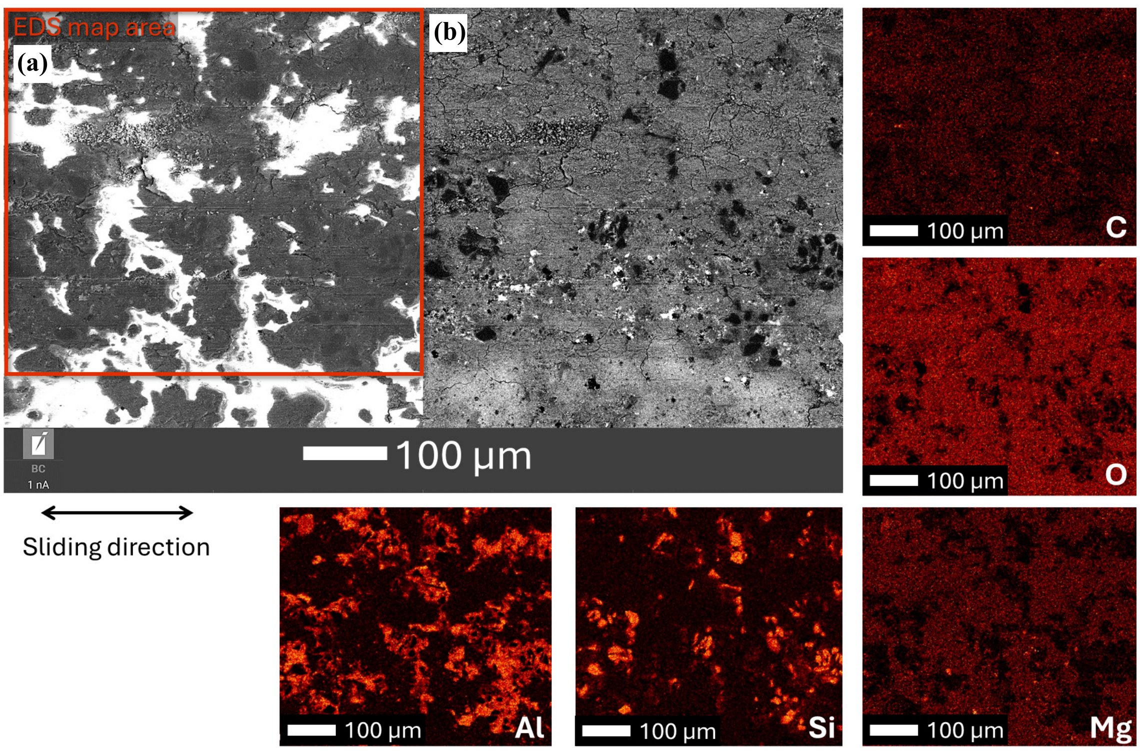

Fig. 10 EDS map analysis of wear track on Mat70: (a) SE and (b) BSE images of the same region of interest.

https://doi.org/10.26599/FRICT.2026.9441217

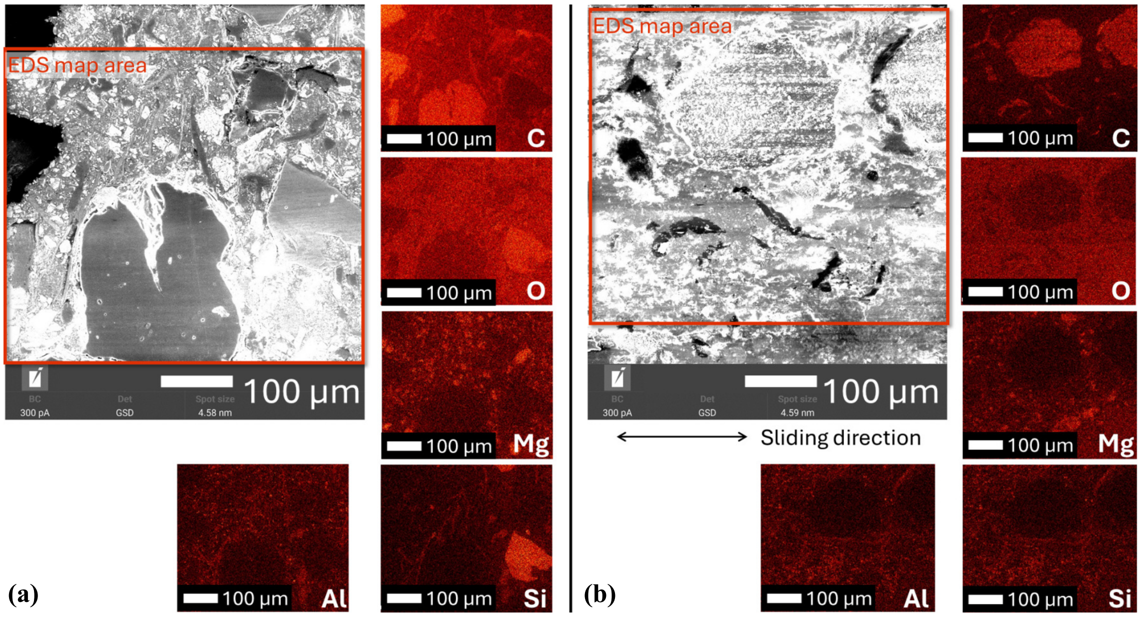

Fig. 11 Brake pad material (a) before and (b) after wear testing against Mat100 with related EDS maps.

and the pins clarifies that for the Al-MMCs there is material transfer from the brake pad to the disc in the form of compacted wear debris that adheres to the disc surface. The layer of transferred material does not cover the entire surface of the wear track, and uncovered areas remain the base material which presents abrasive wear features.

On the GCI surface, the wear tracks and cracks are visible on the entire surface and residuals of powdered wear debris are found inside the wide portions of the cracks. The material transfer from the brake pad to the disc is minimal. These observations align with the wear rate results shown in Fig. 4, suggesting that the material transfer on the Al-MMCs determines the milder wear on the disc samples, hindering the advancing of material loss at the expense of the brake pad. The CoF development in Fig. 3 can be interpreted as a fast development of the transfer layer, which leads to a constant CoF of 0.4–0.45 already in the running-in period that continues during the steady state. Interrupted wear tests are needed to clarify the formation mechanism of the transfer layer. The GCI suffers material loss because there is no development of a transfer layer on the disc surface; therefore, the pin shows a lower wear rate than the Al-MMC equivalents.

4 Conclusions

This study used a pin-on-disc tribometer placed in a one-way ventilated box to investigate the friction, wear, and BWP emissions from Al–SiCp MMC brake discs with various fractions of secondary aluminum in the matrix (i.e., 50%, 70%, and 100%). A GCI brake disc was tested as a reference. PNC down to 4 nm and particle size distribution within the range of 0.25–10 μm were measured with CPC and a portable wide-range aerosol spectrometer (MiniWRAS). Major conclusions can be drawn as follows.

(1) Al–SiCp MMC brake discs showed a clear running-in period and steady state, similar to the GCI brake disc in terms of CoF measurement. The steady-state CoFs of all three Al–SiCp MMCs were stable between 0.4 and 0.45, well within the typical CoF range of brake materials.

(2) Al–SiCp MMC brake discs exhibited apparently milder wear since some worn materials were transferred and adhered to the MMC disc surfaces after testing. Al–SiCp MMC brake discs resulted in a higher wear rate for the mating pins than the traditional GCI brake disc, and the wear rate gradually increased with increasing fraction of secondary aluminum in the matrix.

(3) In the running-in periods, Al–SiCp MMC mainly generated particles within the range of 0.25–3 μm. In the steady state, however, a higher proportion of particles smaller than 0.25 μm was emitted from Al–SiCp MMC discs. It was the opposite for GCI brake discs.

(4) In the steady state, both GCI and Al–SiCp MMC brake discs had a monomodal number-weighted particle size distribution with the mode size approximately 0.5 μm within the measurement range of this study.

(5) Microscopy investigations on the wear tracks clarified the development of a transfer layer from the brake pad to the Al–SiCp MMC discs, resulting in the milder wear for the Al–SiCp MMC brake discs. Consequently, the brake pad showed a higher wear rate than the one tested against the GCI brake disc. This transfer layer built up with the wear debris seemed to be the reason for the reduced BWP emissions from Al–SiCp MMC brake discs.

(6) More advanced particle samplers which can reach the nanosized particle size range and more severe testing conditions (higher contact pressures, higher speeds, and higher temperatures) are recommended for future studies.

Acknowledgements

The authors appreciate the financial support from Vinnova (Swedish Innovation Agency) through the Metalliska Material Strategic Innovation Program (grant number 2022-00828 MaReAl project) and Energimyndigheten (Swedish Energy Agency) through the FFI Program (grant number P2022-00954 SUPERCOAT project). This research also received funding from Stiftelsen för kungskaps-och kompetensutveckling (KK-Stiftelsen) for ProForAl project (grant number 20200217), Swedish Research Council for Sustainable Development (FORMAS) for Nescup project (grant number 2020-02302) and Swedish Research Council (VR) for BrakeMet project (grant number 2025-04737).

Declaration of competing interest

The authors have no competing interests to declare that are relevant to the content of this article.

References

[1] Lyu Y Z, Varriale F, Malmborg V, Ek M, Pagels J, Wahlström J. Tribology and airborne particle emissions from grey cast iron and WC reinforced laser cladded brake discs. *Wear* **556–557**: 205512 (2024)

[2] Manoj A, Saurabh A, Narala S K R, Saravanan P, Natu H P, Verma P C. Surface modification of grey cast iron by laser cladding for automotive brake disc application. *Wear* **532**: 205099 (2023)

[3] Wank A, Schmengler C, Krause A, Müller-Roden K, Wessler T. Environmentally friendly protective coatings for brake disks. *J Therm Spray Techn* **32**: 443–455 (2023)

[4] Verma A S, Sumankant, Suri N M, Yashpal. Corrosion behavior of aluminum base particulate metal matrix composites: A review. *Mater Today Proc* **2**(4–5): 2840–2851 (2015)

[5] Du A D, Lattanzi L, Jarfors A E W, Zheng J C, Wang K K, Yu G G. Role of matrix alloy, reinforcement size and fraction in the sliding wear behaviour of Al–SiCp MMCs against brake pad material. *Wear* **530–531**: 204969 (2023)

[6] Howell G J, Ball A. Dry sliding wear of particulate-reinforced aluminium alloys against automobile friction materials. *Wear* **181**: 379–390 (1995)

[7] Uyyuru R K, Surappa M K, Brusethaug S. Effect of reinforcement volume fraction and size distribution on the tribological behavior of Al-composite/brake pad tribo-couple. *Wear* **260**(11–12): 1248–1255 (2006)

[8] Uyyuru R K, Surappa M K, Brusethaug S. Tribological behavior of Al–Si–SiCp composites/automobile brake pad system under dry sliding conditions. *Tribol Int* **40**(2): 365–373 (2007)

[9] Zheng K L, Wei X S, Yan B, Yan P F. Ceramic waste SiC particle-reinforced Al matrix composite brake materials with a high friction coefficient. *Wear* **458–459**: 203424 (2020)

[10] Zhang S Y, Qu S G, Li Y Y, Chen W P. Two-body abrasive behavior of brake pad dry sliding against interpenetrating network ceramics/Al-alloy composites. *Wear* **268**(7–8): 939–945 (2010)

[11] Zhang S Y, Wang F P. Comparison of friction and wear performances of brake material dry sliding against two aluminum matrix composites reinforced with different SiC particles. *J Mater Process Tech* **182**(1–3): 122–127 (2007)

[12] Shorowordi K M, Haseeb A S M A, Celis J P. Velocity effects on the wear, friction and tribochemistry of aluminum MMC sliding against phenolic brake pad. *Wear* **256**(11–12): 1176–1181 (2004)

[13] Laden K, Guérin J D, Watremez M, Bricout J P. Frictional characteristics of Al–SiC composite brake discs. *Tribol Lett* **8**(4): 237–247 (2000)

[14] Daoud A, Abou El-khair M T. Wear and friction behavior of sand cast brake rotor made of A359–20 vol% SiC particle composites sliding against automobile friction material. *Tribol Int* **43**(3): 544–553 (2010)

[15] Shivamurthy R C, Surappa M K. Tribological characteristics of A356 Al alloy–SiCP composite discs. *Wear* **271**(9–10): 1946–1950 (2011)

[16] Natarajan N, Vijayarangan S, Rajendran I. Wear behaviour of A356/25SiC_p aluminium matrix composites sliding against automobile friction material. *Wear* **261**(7–8): 812–822 (2006)

[17] Shorowordi K M, Haseeb A S M A, Celis J P. Tribo-surface characteristics of Al–B_4C and Al–SiC composites worn under different contact pressures. *Wear* **261**(5–6): 634–641 (2006)

[18] Anoop S, Natarajan S, Kumaresh Babu S P. Analysis of factors influencing dry sliding wear behaviour of Al/SiCp–brake pad tribosystem. *Mater Design* **30**(9): 3831–3838 (2009)

[19] Du A D, Lattanzi L, Jarfors A W E, Zheng J C, Wang K K, Yu G G. On the hardness and elastic modulus of phases in SiC-reinforced Al composite: Role of La and Ce addition. *Materials* **14**(21): 6287 (2021)

[20] Du A D, Lattanzi L, Jarfors A E W, Zhou J, Zheng J C, Wang K K, Yu G G. The influence of Ce, La, and SiC particles addition on the formability of an Al–Si–Cu–Mg–Fe SiCp–MMC. *Materials* **15**(11): 3789 (2022)

[21] Lattanzi L, Etienne A, Li Z Y, Manjunath T, Nixon N, Jarfors A E W, Awe S A. The influence of Ni and Zr additions on the hot compression properties of Al–SiCp composites. *J Alloy Compd* **905**: 164160 (2022)

[22] Lattanzi L, Awe S A. Thermophysical properties of Al-based metal matrix composites suitable for automotive brake discs. *J Alloys Metall Syst* **5**: 100059 (2024)

[23] Lattanzi L, Etienne A, Li Z Y, Chandrashekar G T, Gonapati S R, Awe S A, Jarfors A E W. The effect of Ni and Zr additions on hardness, elastic modulus and wear performance of Al–SiCp composite. *Tribol Int* **169**: 107478 (2022)

[24] Nakanishi H, Kakihara K, Nakayama A, Murayama T. Development of aluminum metal matrix composites (Al-MMC) brake rotor and pad. *JSAE Rev* **23**(3): 365–370 (2002)

[25] Blau P J, Meyer H M. Characteristics of wear particles produced during friction tests of conventional and unconventional disc brake materials. *Wear* **255**(7–12): 1261–1269 (2003)

[26] Djafri M, Bouchetara M, Busch C, Weber S. Effects of humidity and corrosion on the tribological behaviour of the brake disc materials. *Wear* **321**: 8–15 (2014)

[27] Jang H, Ko K, Kim S J, Basch R H, Fash J W. The effect of metal fibers on the friction performance of automotive brake friction materials. *Wear* **256**(3–4): 406–414 (2004)

[28] Ferraris M, Gili F, Lizarralde X, Igartua A, Mendoza G, Blugan G, Gorjan L, Casalegno V. SiC particle reinforced Al matrix composites brazed on aluminum body for lightweight wear resistant brakes. *Ceram Int* **48**(8): 10941–10951 (2022)

[29] Grigoratos T, Martini G. Brake wear particle emissions: A review. *Environ Sci Pollut R* **22**: 2491–2504 (2015)

[30] Lyu Y, Wahlström J, Tu M, Olofsson U. A friction, wear and emission tribometer study of non-asbestos organic pins sliding against AlSiC MMC discs. *Tribol Ind* **40**(2): 274–282 (2018)

[31] Cui J R, Roven H J. Recycling of automotive aluminum. *T Nonferr Metal Soc* **20**(11): 2057–2063 (2010)

[32] Das S K, Yin W M. The worldwide aluminum economy: The current state of the industry. *JOM* **59**: 57–63 (2007)

[33] Lattanzi L, Jarfors A E W, Awe S A. On the possibility of using secondary alloys in the production of aluminum-based metal matrix composite. *Crystals* **14**(4): 333 (2024)

[34] Awe S A, Thomas A. The prospects of lightweight SICAlight discs in the emerging disc brake requirements. In: Proceedings of EuroBrake, 2021.

[35] Wahlström J, Lyu Y Z, Matjeka V, Söderberg A. A pin-on-disc tribometer study of disc brake contact pairs with respect to wear and airborne particle emissions. *Wear* **384**: 124–130 (2017)

[36] zum Hagen F H F, Mathissen M, Grabiec T, Hennicke T, Rettig M, Grochowicz J, Vogt R, Benter T. Study of brake wear particle emissions: Impact of braking and cruising conditions. *Environ Sci Technol* **53**(9): 5143–5150 (2019)

[37] Federici M, Menapace C, Mancini A, Straffelini G, Gialanella S. Pin-on-disc study of dry sliding behavior of Co-free HVOF-coated disc tested against different friction materials. *Friction* **9**: 1242–1258 (2021)

[38] Carlevaris D, Varriale F, Wahlström J, Menapace C. Pin-on-disc tribological characterization of single ingredients used in a brake pad friction material. *Friction* **12**: 2576–2593 (2024)

[39] Wahlström J, Söderberg A, Olander L, Jansson A, Olofsson U. A pin-on-disc simulation of airborne wear particles from disc brakes. *Wear* **268**(5–6): 763–769 (2010)

[40] Underwood E E. Quantitative stereology for microstructural analysis. In: *Microstructural Analysis: Tools and Techniques*. McCall J L, Mueller W M, Eds. New York (USA): Springer, 1973: 35–66.

[41] Kral M V. A crystallographic identification of intermetallic phases in Al–Si alloys. *Mater Lett* **59**(18): 2271–2276 (2005)

[42] Elsharkawi E A, Abdelaziz M H, Doty H W, Valtierra S, Samuel F H. Effect of β-Al_5FeSi and π-$Al_8Mg_3FeSi_6$ phases on the impact toughness and fractography of Al–Si–Mg-based alloys. *Int J Metalcast* **12**: 148–163 (2018)
[43] Archard J F, Hirst W. The wear of metals under unlubricated conditions. *P Roy Soc Lond A Mat* **236**(1206): 397–410 (1956)
[44] Varriale F, Carlevaris D, Wahlström J, Malmborg V, Lyu Y Z. On the impact of pad material ingredients on particulate wear emissions from disc brakes. *Results Eng* **19**: 101397 (2023)
[45] Shen M X, Li H X, Du J H, Ji D H, Liu S P, Xiao Y L. New insights into reducing airborne particle emissions from brake materials: Grooved textures on brake disc surface. *Tribol Int* **174**: 107721 (2022)
[46] Perricone G, Matějka V, Alemani M, Wahlström J, Olofsson U. A test stand study on the volatile emissions of a passenger car brake assembly. *Atmosphere* **10**(5): 263 (2019)
[47] Mathissen M, Grochowicz J, Schmidt C, Vogt R, Farwick zum Hagen F H, Grabiec T, Steven H, Grigoratos T. A novel real-world braking cycle for studying brake wear particle emissions. *Wear* **414**: 219–226 (2018)
[48] Hesse D, Hamatschek C, Augsburg K, Weigelt T, Prahst A, Gramstat S. Testing of alternative disc brakes and friction materials regarding brake wear particle emissions and temperature behavior. *Atmosphere* **12**(4): 436 (2021)
[49] Nosko O, Olofsson U. Effective density of airborne wear particles from car brake materials. *J Aerosol Sci* **107**: 94–106 (2017)
[50] Lyu Y Z, Sinha A, Olofsson U, Gialanella S, Wahlström J. Characterization of ultrafine particles from hardfacing coated brake rotors. *Friction* **11**: 125–140 (2023)
[51] Lyu Y Z, Leonardi M, Wahlström J, Gialanella S, Olofsson U. Friction, wear and airborne particle emission from Cu-free brake materials. *Tribol Int* **141**: 105959 (2020)
[52] Park J, Joo B, Seo H, Song W S, Lee J J, Lee W K, Jang H. Analysis of wear induced particle emissions from brake pads during the worldwide harmonized light vehicles test procedure (WLTP). *Wear* **466–467**: 203539 (2021)
[53] Giechaskiel B, Grigoratos T, Dilara P, Karageorgiou T, Ntziachristos L, Samaras Z. Light-duty vehicle brake emission factors. *Atmosphere* **15**(1): 97 (2024)

Yezhe Lyu is currently an associate professor at the Department of Industrial and Mechanical Engineering Sciences, Lund University, Sweden. He obtained his Ph.D. degree in machine design at KTH Royal Institute of Technology, Sweden, in 2018. He was a JSPS Fellow visiting Keio University in 2020. His current research focuses on innovative materials to reduce wear particle emissions from non-exhaust sources such as brakes, tires, roads, wheel–rail contact, etc., with financial support from the Swedish Research Council, the Swedish Energy Agency, etc.

Lucia Lattanzi is an associate professor and senior lecturer at the Department of Materials and Manufacturing, School of Engineering, Jönköping University, Sweden. She obtained her Ph.D. degree in materials engineering at University of Ferrara in 2019. Her research interests are the performance and production of aluminum-based alloys and their composites. She has been awarded a series of research projects by the Swedish Knowledge Foundation and the Swedish Innovation Agency.

Samuel Awe obtained his Ph.D. degree in process metallurgy at Luleå University of Technology, Sweden, in 2013. He is acting as senior materials & metallurgical engineering and research manager at Volvo Cars Propulsion Components. He focuses on the innovation on brake materials, especially brake discs in order to increase the performance under extreme conditions with lower environmental impacts. He is leading and participating a series of research projects funded by the Swedish Innovation Agency, the European Institute of Innovation & Technology, etc.

Anders EW Jarfors is a full professor in materials and manufacturing–casting at the Department of Materials and Manufacturing, Jönköping University, Sweden. His research area includes technology for the manufacture of cast components, both the process chain as they finished their structure and properties, as well as phenomena that are of importance for its quality. His particular focus is on material properties during the manufacturing process, and the finished component. His research is largely funded by Swedish Industries and National Foundations such as the Swedish Innovation Agency and the Swedish Knowledge Foundation.

Jens Wahlström is chair professor in machine elements at the Department of Industrial and Mechanical Engineering Sciences, Lund University, Sweden. He is an excellent teaching practitioner and a committee member of the research programme board at the university. His research focuses on tribological performance and non-exhaust emissions from machine elements (such as brakes, clutches, tire–road, and wheel–rail) in road and rail vehicles. He has designed and applied both experimental and simulation methods in his research. His research is supported by the European Union Framework 7 and Horizon 2020 programmes, the Swedish Research Council, the Swedish Innovation Agency, and other funding sources.